HHS Public Access

Author manuscript

Magn Reson Med. Author manuscript; available in PMC 2022 April 01.

Quantitative and simultaneous measurement of oxygen consumption rates in rat brain and skeletal muscle using ^{17}O MRS imaging at 16.4T

Hannes M. Wiesner[1,2], **Dávid Z. Balla**[1], **Klaus Scheffler**[1,3], **Kâmil Uğurbil**[2], **Xiao-Hong Zhu**[2], **Wei Chen**[2], **Kâmil Uludağ**[4,5,*], **Rolf Pohmann**[1,*,†]

[1]High-Field Magnetic Resonance Center, Max Planck Institute for Biological Cybernetics, 72076 Tübingen, Germany

[2]Center for Magnetic Resonance Research, Department of Radiology, University of Minnesota Medical School, Minneapolis, MN 55455, USA

[3]Department of Biomedical Magnetic Resonance, Eberhard Karls University of Tübingen, 72076 Tübingen, Germany

[4]Techna Institute & Koerner Scientist in MR Imaging, University Health Network, Toronto, ON, Canada

[5]Center for Neuroscience Imaging Research, Institute for Basic Science & Department of Biomedical Engineering, Sungkyunkwan University, Suwon, South Korea

Abstract

Purpose: Oxygen-17 MRS imaging, successfully used in the brain, is extended by imaging the oxygen metabolic rate in the resting skeletal muscle and to determine the total whole-body oxygen metabolic rate in the rat.

Methods: During and after inhalations of $^{17}O_2$ gas, dynamic ^{17}O MRSI was performed in rats (n=8) ventilated with N_2O or N_2 at 16.4T. Time courses of the $H_2{}^{17}O$ concentration from regions-of-interest located in brain and muscle tissue were examined and used to fit an animal-adapted three-phase metabolic model of oxygen consumption. Cerebral blood flow (CBF) was determined with an independent washout method. Finally, body oxygen metabolic rate was calculated using a global steady-state approach.

Results: Cerebral metabolic rate of oxygen consumption ($CMRO_2$) was 1.97 ± 0.19 μmol/g/min on average. The resting metabolic rate of oxygen consumption in skeletal muscle ($RMRO_2$) was 0.32 ± 0.12 μmol/g/min, and > 6 times lower than $CMRO_2$. Global oxygen consumed by the body

[†]Corresponding Author: Dr. Rolf Pohmann, High-Field Magnetic Resonance Center, Max Planck Institute for Biological Cybernetics, Max-Planck-Ring 11, 72076 Tübingen, Germany, Phone: +49 7071 601 903, Fax: +49 7071 601 702, rolf.pohmann@tuebingen.mpg.de.

[*]Authors Kâmil Uludağ and Rolf Pohmann contributed equally to this work.

Supporting Information Figure S1 A,B: Zoomed views of the signal time courses around the beginning (A) and end (B) of the inhalation, for different values also show the different time points as with the different resolution protocols (10 s vs. 30 s per CSI volume, with the latter in close resemblance to the experimental design in Ref. 4 [42 s per 3D CSI volume]). The low ρ_{human} causes a substantially delayed reaction at both beginning and end of the inhalation, with less effect at an increase of a hypothetical 7 min^{-1}.

(VO_2) was 24.2 ± 3.6 ml O_2/kg body weight/min. CBF was estimated to be 0.28 ± 0.02 ml/g/min and 0.34 ± 0.06 ml/g/min for the N_2 and N_2O ventilation condition, respectively.

Conclusion: We have evaluated the feasibility of ^{17}O MRSI for imaging and quantifying the oxygen consumption rate in low metabolizing organs such as the skeletal muscle at rest. Additionally, we have shown that CBF is slightly increased in the case of ventilation with N_2O. We expect this study to be beneficial to the application of ^{17}O MRSI to a wider range of organs, though further validation is advised.

Keywords

Mitochondrial water and $H_2{}^{17}O$; oxygen-17 MRS imaging (^{17}O MRSI); Cerebral metabolic rate of oxygen ($CMRO_2$); Cerebral blood flow (CBF); Skeletal muscle; Muscle resting metabolic rate of oxygen consumption ($RMRO_2$); Cerebrovascular Circulation; Basal body metabolic rate of oxygen (VO_2)

Introduction

Noninvasively measuring cellular oxygen metabolism using $^{17}O_2$ tracer and in vivo ^{17}O spectroscopic imaging (^{17}O MRSI) at ultrahigh field (UHF) is a promising tool for studying cellular energy metabolism and physiology.[1] The ^{17}O imaging approach allows to quantify the cerebral metabolic rate of oxygen ($CMRO_2$) in human[2] and animal brain.[3–5] Although imaging studies have been performed to differentiate the cerebral metabolic rates between gray and white matter with ^{17}O,[2,6,7] few measurements were done outside the brain,[8–10] often focusing on aerobic organs with a high metabolic rate. Obviously lower metabolic rates, such as in resting muscle tissues, result in slower turnover rates from $^{17}O_2$ to $H_2{}^{17}O$ in the mitochondria. Thus, less labeled $H_2{}^{17}O$ signal in tissue could necessitate longer scans or require more application of ^{17}O-isotope labeled O_2 to achieve an adequate signal-to-noise ratio (SNR) for imaging. The dynamics of $H_2{}^{17}O$ signal change as well as a uncertainty in modeling with resulting longer inhalation durations is affected by blood perfusion and recirculation. This unmet challenge motivates our investigation of the feasibility of imaging the low oxygen metabolic rate in resting skeletal muscle using ^{17}O MRSI in simultaneous comparison to the brain oxygen metabolism rates in the same subject. By using significantly longer $^{17}O_2$ inhalation times, the amount of generated $H_2{}^{17}O$ in biological tissues and the resulting ^{17}O MR signal is largely increased and even more so by multiple inhalations,[7,11] allowing to reliably observe metabolic and perfusion[12] parameters at increased sensitivity. However, in advantage to ^{15}O PET no subtraction scans have to be performed for the subtraction of gaseous oxygen signal.[13–16]

In this study, we simultaneously acquired dynamic time courses of $H_2{}^{17}O$ signals in brain and muscle tissue in rats during $^{17}O_2$ inhalations using three-dimensional (3D) ^{17}O MRSI at an ultrahigh magnetic field of 16.4 Tesla (T). Repetitive and longer inhalations of $^{17}O_2$ gas than in previous measurements in rodents resulted in a large increase of the $H_2{}^{17}O$ concentration several times above natural abundance. The $H_2{}^{17}O$ dynamic signals were fitted with two commonly used models: a three-phase metabolic model using to the whole $H_2{}^{17}O$ dynamic time course, acquired before, during and after inhalations to determine the metabolic rates of oxygen consumption[2], and a washout model was applied to the post-

inhalation brain data to estimate the cerebral blood flow (CBF).[12] The three-phase metabolic model, which was previously used in human brain gray and white matter, was modified to obtain the low resting-state metabolic rate of oxygen consumption in the rat skeletal muscle (Muscle $RMRO_2$) for exploring the feasibility using the ^{17}O MRSI method in other tissues. The washout technique, allowing for estimation of CBF, as previously validated in rodent brain, was used to investigate two groups of rats ventilated with different blends of gases (oxygen with N_2 or N_2O). Finally, recirculation of $H_2{}^{17}O$ leading to a new equilibrium at the end of the post-inhalation period was observed and employed to estimate the organism's global metabolism rate (i.e., total body oxygen expenditure VO_2), which was then compared to the regional metabolic rates of oxygen consumption.

Theory

Three-phase model adaptation

A previously published model for determining the human brain oxygen metabolism rate[2] fitting three phases of a $H_2{}^{17}O$ time course (Phase 1: before, Phase 2: during and Phase 3 after an $^{17}O_2$ inhalation) was adapted to the rat systemic characteristics. We chose this model for the study in rodents since it applies well to low metabolic rates involving a significant amount of recirculating $H_2{}^{17}O$. In particular with longer inhalations, cardiopulmonary factors like the cardiac output are increasingly important.[2]

The time dependent brain tissue $H_2{}^{17}O$ concentration defined as molar volume $M_V^{H_2^{17}O}{}_{(t)}$ in an imaging voxel can be described as (refer to Eqn. [2] in Reference 2 for more details):

$$\frac{dM_V^{H_2^{17}O}(t)}{dt} = 2 \cdot CMRO_2 \cdot A^{17}{}_{O_2}(t) - K_L \cdot M_V^{H_2^{17}O}(t) + K_G \cdot B^{H_2^{17}O}(t)\,. \quad [1]$$

The three terms on the right side of Eqn. [1] can be separated into: 1) the regional metabolic activity producing $H_2{}^{17}O$ (i.e., the cerebral metabolic rate of oxygen consumption: $CMRO_2$), depending on the arterial ^{17}O-isotope enrichment [$A^{17}{}_{O_2}$] of oxygen gas delivered through hemoglobin; 2) the loss [K_L] of $H_2{}^{17}O$ mainly due to (cerebral) blood flow or perfusion washout into the draining venous vascularity; and 3) the gain [K_G] of $H_2{}^{17}O$ through inflow of blood [$B^{H_2^{17}O}$] containing $H_2{}^{17}O$, recirculating from both local metabolizing tissue and whole body oxygen metabolism.

By integration over time, Eqn. [1] can be used to fit the time courses (see Eqn. [6] in Reference 2) of $H_2{}^{17}O$ signal for each imaging voxel to derive the oxygen metabolic rate (MRO_2) in brain or muscle tissue (as $CMRO_2$ or $RMRO_2$). We propose herein that, in principle, for any sufficiently perfused organ, oxygen consumption rates even below the systemic global aerobic rate (VO_2) can be measured. The quantification is simplified if the water content of the imaged tissue, which can be calibrated by the $H_2{}^{17}O$ natural abundance concentration and the ^{17}O signal measured in Phase 1, is known.[3–5] The water content of muscle and brain can be approximated by assuming comparability to humans (i.e., mice[17]:

74.4% wt in muscle vs. human:[18] 79.5% wt in striated muscle and 73.3% wt in brain). Furthermore, the tissue density for rodents (1.06 kg/liter for skeletal muscle[19]) was employed for unit conversion. Eqn. [1] can then be used to determine the oxygen metabolic rates of the rodent muscle and brain.

Systemic oxygen expenditure VO_2

The total body oxygen expenditure or metabolic rate (VO_2 in the unit of μmol/g body weight/min) can be defined as the cumulative amount of metabolic $H_2{}^{17}O$ added to the organism by inhalation and metabolism of $^{17}O_2$ tracer with a fixed enrichment within a given inhalation time. The average body oxygen metabolic rate ($VO_{2,average}$) per minute can then be determined using the equilibrium $H_2{}^{17}O$ signal in tissue measured during the late part of the post-inhalation period (Phase 3) assuming that a new equilibrium (or steady state of the tissue $H_2{}^{17}O$ signal) has been established:

$$VO_2 = \frac{M_V^{H_2^{17}O}(equilibrium)}{t_{inhalation} \times f} = VO_{2,\,average} \;/\; f \;(\mathrm{t} > > \mathrm{t}_{\mathrm{inhalation}}) \qquad [2]$$

$t_{inhalation}$ is the inhalation duration; $M_V^{H_2^{17}O}(equilibrium)$ is the average tissue $H_2{}^{17}O$ concentration ($M_V^{H_2^{17}O}$) at equilibrium (in this study, ~3 inhalation durations after $^{17}O_2$ inhalation) when its pre-inhalation level is set to zero; the conventional format of VO_2 in volume of oxygen gas is usually given in ml/kg body weight/min and requires a unit conversion f by division of 0.0446 $\mu mol^{-1}ml$.[20]

Methods

Simulation of circulation impact and metabolic rate on the $H_2{}^{17}O$ time courses

Inhalations with a $^{17}O_2$ enrichment of 70% were simulated using the previously outlined three-phase model for two settings: 1) simulation with a fixed high metabolic rate (i.e. isometabolic $CMRO_2$=2 μmol/g/min) varying only the circulatory parameters (K_G and K_L) in ranges reported in the literature[2,6,9,21,7] (Phase 2 with 15.25 min inhalation duration); and 2) simulation of varying metabolic rate and corresponding changes in perfusion. In the second stage simulation, different levels of local oxygen metabolic rates were set (MRO_2=2; 1; 0.5; 0 μmol/g/min) with fixed parameters K_L=0.2 and K_G=0.3, unless otherwise noted, during an inhalation using Eqn. [1] to qualitatively assess the time dependence of the tissue $H_2{}^{17}O$ signal. Specifically this allowed investigation under idealized conditions of the transitions between phases of the model.[2]

Furthermore, we adapted and evaluated the rodent specific systemic parameter (ρ_{rat}) as detailed in the Supporting Information.

Animal preparation and physiology monitoring

All procedures and experiments were approved by the local authorities (Regierungspräsidium) and were in compliance with the guidelines of the European

Community (EUVD 86/609/EEC) for the care and use of laboratory animals. A total of 8 male Wistar rats (Charles River Laboratories, Sulzfeld, Germany) were used in this study (Table 1, mean body weight 312 ± 93 g). Artificial ventilation and maintenance of physiological stability is also further described in detail in the Supporting Information.

Ventilation mixtures with enriched $^{17}O_2$ gas (Oxygen gas fraction ~25-35% with 70% enriched $^{17}O_2$ Nukem GmbH, Germany) were prepared in non-diffusive gas bags (Hans Rudolph, Inc., Shawnee KS, USA). Oxygen was mixed with N_2 in one group (Table 1, animals A-D, n=4) and with N_2O in a second group of animals (Table 1, animals E-H, n=4). At the end of each experiment, the animals were euthanized followed by post-mortem imaging as previously reported.[22]

MRI instrumentation and data acquisition

Magnetic resonance imaging was performed on a BioSpec Avance III system (Bruker Biospin MRI GmbH, Ettlingen, Germany) using a 26 cm bore 16.4 Tesla magnet and gradients with 12 cm inner diameter, 1 T m^{-1} maximum strength and 212 μs ramp time (Resonance Research Inc., Billerica, MA, USA). Custom-built quadrature surface coils (elliptical loops each ~1.5×1.2 cm) were tuned to the ^{17}O Larmor-frequency (94.6 MHz) for ^{17}O imaging and a separate ^{1}H butterfly RF coil passively decoupled from the ^{17}O coils was used. Anatomical ^{1}H MRI FLASH images with TR=2 s, TE=10 ms (nt=4 averages), 59×59 μm^2 in-plane resolution and 29 axial slices (thickness=1 mm) were acquired within 25 min 36 s.

A k-space acquisition-weighted 3D CSI pulse sequence was used for all ^{17}O MRSI acquisitions. Two types of time-series were acquired for each rat: natural abundance tissue $H_2{}^{17}O$ signal before any $^{17}O_2$ gas inhalation for calibration of $H_2{}^{17}O$ concentration in each CSI voxel, and during and after a single or repeated inhalation for metabolic rate and CBF analysis. In all in vivo ^{17}O MRSI acquisitions, we used a field of view (FOV) of 27.5×12.5×18 mm^3, spectroscopic sampling points 375, and acquisition duration of 3.75 ms with a delay of 0.538 ms from an excitation RF pulse. TR was 4.92 ms, optimized for tissue T_2*,[23] and RF-excitation was performed with a 68° hard pulse of 200 μs duration.

In the majority of animals (Table 1, animals A-F, referred to as “high-resolution protocol”) the FOV was scanned by an acquisition matrix of 15×7×7, resulting in a voxel volume of 43.1 μl as defined by the width of the spatial response function (SRF).[24–26] Each 3D ^{17}O CSI volume was acquired within 30.2 s, with a maximum number of averages nt_{max}=74 at the k-space center (a total of 6144 FIDs or 735 k-space points per CSI volume). Fifty natural abundance $H_2{}^{17}O$ CSI were acquired within ~25 min at baseline, and a total of 109 volumes per full inhalation, started shortly before it, were collected within 54 min 57 s (see Table 1 for individual inhalation durations) including a ~38 min long post-inhalation acquisition (i.e., the $H_2{}^{17}O$ washout period).

In a subgroup of 2 animals (Table 1, animals G & H, referred to as “low-resolution protocol”), the same FOV was scanned with an acquired matrix of 9×7×7, leading to a voxel size of 77.3 μl by SRF adjustment with nt_{max}=45 averages at the k-space center (a total of 2048 FIDs or 441 k-space points per CSI volume) and 10.1 s acquisition per 3D CSI

volume. Natural abundance $H_2{}^{17}O$ CSI volumes (n=50) were acquired within ~8 mins 24 s and the same acquisition duration of 54 min 57 s was used to acquire 327 volumes of inhalation data. Other acquisition parameters remained the same.

Post-mortem CSI-acquisitions were performed without k-space weighting (12 ms TR and 70° flip angle) and with a pulse length of 400 μs. A FOV of 27.5×12.5×25 mm^3 was sampled with a matrix of 41×19×25 voxels (nominal voxel size 0.44 μl). Approximately a total of 2.5 million FIDs with 1000 points each and a spectral bandwidth of 100 kHz were acquired in 8 h 18 min.

Brain co-registration and tissue selection

The 3D ^{17}O-CSI data were co-registered with ^{1}H anatomic images and high resolution (post-mortem) $H_2{}^{17}O$ images with the same FOV as illustrated in Figures 1A–C. Equally-sized regions of interest (ROI) were selected (−3 mm Bregma)[27] for brain and in lateral muscle compartments in the same coronal slices. The topography of the temporalis muscle was verified anatomically[28–30] and left and right lateral ROIs (42.4 μl, n=40 voxels after zero-filling in animals A-F, 49.4 μl, n=28 voxels after zero-filling in animals G-H) were chosen as a subset of the temporalis volume (0.422 ml)[31] carefully avoiding partial volume contamination from adjacent brain tissue.

Post processing, in vivo T_2* estimation and metabolic fitting

Acquired CSI datasets were Fourier-transformed and the peak of the magnitude spectrum of $H_2{}^{17}O$ after apodization (T_2* = 1.8 ms in time domain) was normalized to the natural abundance $H_2{}^{17}O$ concentration of 16.3 μmol/g wet tissue of both muscle and brain, assuming equal $H_2{}^{17}O$ concentrations (i.e., water content) in muscle and brain tissue[18,32–34]. Calibration was performed through normalization from the previously defined natural abundance acquisitions of each rat, last 20 CSI volumes for the high resolution protocol, 40 volumes for low resolution, and pre-inhalation time points (Phase 1) were 12 CSI volumes and 23 volumes, respectively. Signals were smoothed by a nearest neighbor moving average (three adjacent CSI time points).[7]

Separately, for each rat, the data of two rats in the low and high resolution protocols were phased and the localized semilogarithmic FIDs were fitted against time for in vivo T_2* relaxation measurement as described in detail in Ref. 22.[22]

The metabolic model was fitted according to Eqn. [1] using a non-linear least-squares algorithm (Curve fitting toolbox, Matlab) to the $H_2{}^{17}O$ signal time courses of tissue signal (inhalation time (t) as independent variable; $CMRO_2$ for brain and $RMRO_2$ for muscle, K_G, K_L as dependent variables).

Estimation of CBF

CBF was estimated from the same brain ROIs, only based on the $H_2{}^{17}O$ signal after the end of the inhalation (i.e., ~38 min of washout). The previously validated washout model[12] is based on the return of local $H_2{}^{17}O$ overproduction to a new systemic equilibrium in relation

to the rest of the body (VO_2). The concentration of brain tissue $H_2{}^{17}O$ using mono-exponential fitting against time courses can be described by the following equation:[12,35]

$$Cb(t) = k3 \times exp\frac{CBF \times t}{k_1} + k_4 . \quad [3]$$

The primary decay constant, proportional to CBF/k1, can be converted by multiplication with 1.86 to absolute CBF units of ml/g/min (whereas k3 and k4 are scale factors).[12] Then, the two groups with different ventilation mixtures were compared (N_2 vs. N_2O).

All results are reported in mean ± standard deviation (SD).

Results

Proton structural images showed a clear anatomical contrast between brain and muscle tissue (Figure 1A). Coregistered geometry of ^{17}O contrast in both in vivo (Figure 1B) and ex vivo ^{17}O high-resolution images (Figure 1C) matched the anticipated intensity distribution of the ^{17}O surface coil, i.e., stronger ^{17}O water signal at the surface and in the quadrature B_1 field overlap region in the brain. Figure 2 illustrates representative natural abundance $H_2{}^{17}O$ spectra summed over the ROIs before inhalation from low-resolution (Figure 2A, 10 s acquisition averaging) and high-resolution (Figure 2B, 30 s acquisition averaging) ^{17}O MRSI, indicating a high SNR offered at 16.4T, in particular, in the brain.

Simulation of parameterized $H_2{}^{17}O$ dynamics

The simulation results shown in Figure 3A demonstrate the sensitivity of the parameters of the three-phase model, in particular the K_L or K_G values on the $H_2{}^{17}O$ dynamics, which represents the strong influence of perfusion. Time courses of the simulated ^{17}O signal with varying metabolic rate are shown in Figure 3B for four different metabolic rates, exemplifying representative values for the brain and the muscle.

The simulated metabolic rates at different levels showed a qualitatively distinct shape of the $H_2{}^{17}O$ signal dynamics at low metabolism (i.e., sigmoidal). Despite significant differences in the early Phase 2 (Phase 2A), the slopes converge in a non-linear way during the late Phase 2 (Phase 2B) as shown in Figure 3B. The simulation results indicate that the early dynamic change of the tissue $H_2{}^{17}O$ signal after inhalation of $^{17}O_2$ gas is more sensitive to the local metabolic rate than that of late Phase 2.

A novel observation from this simulation was that the same K_G/K_L ratio leads to the same equilibrium level of $H_2{}^{17}O$ signal at the end of Phase 3 (Figure 3A for brain and 3B for muscle at K_G/K_L ratio = 1.5). This suggests that even if the oxygen metabolic rates vary greatly in different tissues (e.g., brain vs. muscle), the relative contributions of the $H_2{}^{17}O$ signal gain and signal loss due to recirculation and perfusion in different voxels remain the same. Thus, the voxels containing different tissue types will eventually reach the same $H_2{}^{17}O$ concentration level.

Metabolic rate estimates for brain and resting skeletal muscle tissue

As shown in Figure 4, the $H_2{}^{17}O$ signal intensity in muscle ROIs grew in a slower fashion, then accelerated during the late Phase 2 (i.e. Phase 2B) before approaching a saturation after the inhalation ended. An absent $H_2{}^{17}O$ signal decrease in muscle tissue during the post inhalation phase due to competing processes between $H_2{}^{17}O$ recirculation and washout was in stark contrast to the obvious $H_2{}^{17}O$ signal decay observed in the brain ROIs (Figure 4B). Reproducible time courses were observed during three repeated inhalation measurements in the same animal and MR imaging session (Fig. 4C).

Fitting the metabolic rates of brain ROIs, an overall average of $CMRO_2$ = 1.97 ± 0.19 μmol/g/min (n=26 ROIs from all 8 rats) was determined. For the two subgroups consisting of 4 rats each a $CMRO_2$ of 2.07 ± 0.15 (n=14 ROIs) and slightly lower 1.84 ± 0.14 μmol/g/min (n=12 ROIs) were estimated with N_2 and N_2O, respectively (Table 2), and no significant differences between the two hemispheres were detected. In muscle ROIs, an average $RMRO_2$ of 0.32 ± 0.12 μmol/g/min (n=21 ROIs) was determined with some notable intra-subject left and right lateral differences. The estimated muscle oxygen metabolic rates were only a sixth of that of the brain. The perfusion and diffusion related parameter K_G was higher than the parameter K_L for both tissue types (for brain: averaged K_G=0.34 ± 0.05, K_L =0.22 ± 0.03, n=26; and for muscle: K_G=0.63 ± 0.33, K_L=0.40 ± 0.17, n=21). Group averages for brain tissue were K_G=0.34 ± 0.04 (n=14) for N_2 and K_G=0.34 ± 0.07 (n=12) for N_2O without a statistically significant difference. In contrast, K_L=0.20 ± 0.02 (n=14) for brain within the N_2 group was increased by +22% to K_L=0.24 ± 0.02 (n=12) in the N_2O group with statistical significance (two-sided unpaired t-test at $p<0.005$).

The overall ratio of K_G/K_L determined within sessions was 1.51 ± 0.23 (n=21 ROIs) for muscle and 1.58 ± 0.23 (n=26 ROIs) for brain tissue, respectively; no statistically significant difference between the two tissue types was observed. The same K_G/K_L ratios between the brain and muscle converged to the same level of equilibrium $H_2{}^{17}O$ signal at the later Phase 3 (Figure 4B) despite > 6 times of difference in the metabolic rate between the two tissues. This finding is in agreement with the prediction from the simulations shown in Figure 3.

Cerebral blood flow and VO_2 in N_2O vs. N_2 ventilated animals

The estimated average oxygen metabolic rate of the entire body per gram tissue $VO_{2,average}$ according to Eqn. [2] was 1.08 ± 0.20 μmol/g/min (n=13) and 1.08 ± 0.16 μmol/g/min (n=13) as inferred from right and left averaged muscle and brain ROI time courses, respectively (Table 3). Consistent with the conventional unit commonly used in the literature, VO_2 was converted to 24.2 ml/kg body weight/min, derived from the steady-state $H_2{}^{17}O$ signals from both tissue types. Cerebral blood flow in the N_2 ventilated animal brain from average k1 = 0.15 ± 0.01 (n=14) resulted in CBF 0.28 ± 0.02 ml/g/min and significantly elevated CBF (+21%, $p<0.005$ with two-sided unpaired t-test) was observed in the N_2O ventilated group with a mean of 0.34 ± 0.06 ml/g/min (n=12, Table 3).

In vivo T_2* in muscle and brain tissue

Figure 5 shows the lower T_2* of $H_2{}^{17}O$ in muscle tissue and ~40% higher T_2* in brain tissue, that are correlated against the independent metabolic rates in the two types of tissues.

In the same rats a more than 5-fold difference in metabolic rate between muscle and brain is apparent.

Discussion

This study demonstrates three perspectives about the utility of the noninvasive and quantitative ^{17}O MRSI or MRI method with inhalation of $^{17}O_2$ gas determining the oxygen consumption rates in organs with higher and/or lower metabolic activity, measuring the systemic global oxygen consumption rate using a steady-state model, and characterizing local cerebral blood flow under two experimental conditions.

Modeling dynamics of $H_2{}^{17}O$ signal in muscle and brain

We have simulated the $H_2{}^{17}O$ signal dynamics using an animal-adapted three-phase metabolic model as described by Eqn. [1] using different parameter settings to mimic the experimentally measured $H_2{}^{17}O$ time courses (see examples in Figure 3). The simulation data indicate that the initial change of the tissue $H_2{}^{17}O$ signal during the early inhalation period (Phase 2A) is dominated by the metabolically produced $H_2{}^{17}O$ and the contribution from recirculating $H_2{}^{17}O$ is small. Therefore, the initial slope of the $H_2{}^{17}O$ concentration in Phase 2A is sensitive to the oxygen metabolic rate of the tissue,[36] which is much slower in muscle as compared to the steeper increase in brain tissue. Despite the expected differences in the local metabolic rate, the time course of the $H_2{}^{17}O$ signal in the late inhalation phase (Phase 2B) converged to a relatively similar slope for all tissues (see Figures 3, 4 and also Supporting Information Figure S1B). The contribution of recirculating water increased with inhalation time and gradually dominated the $H_2{}^{17}O$ signal in the later phase of the inhalation, resulting in converging slopes between high and low activity tissues as observed in experimental data.

Determining the oxygen metabolic rates in muscle and brain

Despite the limited spatial specificity, arterio-venous difference measurements can still be regarded as the gold standard for oxygen consumption measurements. However, due to their invasiveness they are less convenient and the variability of draining vascular territory effects on reproducibility motivates the use of non-invasive alternatives like ^{17}O MRSI/MRI with $^{17}O_2$ tracer inhalation, as in parallel has been attempted through ^{15}O PET.[37,38] By fitting the $H_2{}^{17}O$ signal dynamics of the rat muscle ROIs to the adapted three-phase metabolic model, the resting-state metabolic rate of oxygen consumption in skeletal muscle ($RMRO_2$) was 0.32 ± 0.12 μmol/g/min. Comparing to the literature reports of oxygen metabolic rates in skeletal muscle from the earliest in vitro estimates[39] to more recent studies [40] in Wistar rats, the results of the present study show a good agreement with the literature values (Table 4). Perfused rat hindquarter muscle metabolic rate was reported similar (e.g., 0.37 μmol O_2/g/min),[41] depending on modality.[42] Other differences could be inherent to the heterogeneity of muscle fibers,[43–46] which in the case of the temporalis muscle is low[30,47] compared to other muscles (e.g., soleus or gastrocnemius) and in other species.[29,47,48] To the best of our knowledge, this study is the first to report measurements of oxygen metabolic rates using ^{17}O MR imaging for resting skeletal muscle, although working cardiac muscle with a high oxygen consumption rate has been shown before in isolated heart[8] as well as in vivo rat

heart[10]. In muscle, alternative pathways (i.e., fatty acids) are possible in contrast to the glucose-based metabolism of the brain[30,31]. However, both are based on of oxygen as the substrate in the predominant mitochondrial electron transfer chain as origin of metabolic $H_2{}^{17}O$. Therefore, this study is in agreement with previous measurements in the cardiac muscle both perfused[8] and in vivo[10], but it extends to a much lower regime of metabolic rates in the immobilized, resting skeletal muscle with very distinguishable characteristics.[2]

The averaged $CMRO_2$ value (= 1.97 ± 0.19 μmol/g/min) as determined in this study is in agreement with the value (= 2.19 ± 0.14 μmol/g/min) from a literature report in the rat brain under relatively lower dose α-chloralose anesthesia obtained with a different modeling and experimental protocol.[3] These comparisons provide strong evidence to support the validity and reliability of the quantitative ^{17}O MRS imaging method as described in this work for noninvasively imaging oxygen metabolic rates in the brain and resting muscle with a very low metabolic activity. Thus, we conclude that the same imaging approach should be applicable for most organs across a wide range of metabolic rates.

Global systemic metabolic rates

It should be reasonable to assume that the metabolite pools are in equilibrium upon a stable physiological condition of the animal.[49] As observed in both simulation and experimental data, the post-inhalation $H_2{}^{17}O$ concentrations of different ROIs containing brain or muscle tissue eventually converged to the same steady-state level, which represented the new equilibrium $H_2{}^{17}O$ concentration after the $^{17}O_2$ inhalation. Based on that information and Eqn. [2], we were able to derive the global systemic metabolic rate. Metabolic inter- or intra-subject fluctuations are likely caused by variations in the physiological animal condition (i.e., ventilation parameters, anesthesia status and body weight). Thus, in contrast to other studies,[7] our estimates of the average global oxygen metabolic rate (Table 3) were robust and consistent, independent of whether they were inferred from brain or muscle ROI time courses. Previous studies have used ^{17}O to assess the total metabolic rate of oxygen so far in dogs[50] and mealworms[51,52]. Very early studies on Wistar rats[39] measured oxygen consumption in muscle in vitro, with more recent reports estimating VO_2 for muscle of 18.7 ml O_2/kg/min in anesthetized rats[53] and 24.5 ± 8.5 ml O_2/kg/min in awake rats of the same strain, remarkably close to our results (24.2 ml O_2/kg/min).[54] The variations in literature values also highlight possible inter-subject variations and different approaches used for these studies.[55–57]

Increased washout of locally produced $H_2{}^{17}O$ during N_2O ventilation

The washout of $H_2{}^{17}O$ in brain tissue during the post-inhalation period (i.e., related to perfusion or CBF) has been established previously.[12] It reflects the dynamics of perfusion washout of the metabolically produced $H_2{}^{17}O$ in brain tissue and an inflow of global recirculating $H_2{}^{17}O$. However, there is no observable “washout” in the lower metabolic muscle tissue ($RMRO_2$ = 0.36 μmol/g/min) below the average body oxygen metabolic rate ($VO_{2,average}$ ~1.1 μmol/g/min), presumably due to a substantial inflow effect from recirculating $H_2{}^{17}O$ and low metabolic activity. Thus, in contrast to brain tissue, a significant extent of “wash in” from systemic recirculation after the $^{17}O_2$ inhalation was observed in muscle (Figure 4, from t=15 min onwards).

An increase in cerebral blood flow through vasodilation has been observed and reported before with high percentage N_2O administration.[58] Thus, the anesthetic properties and vasodilatory effects of N_2O may reduce the global metabolism and possibly uncouple it partially from the narrowly regulated cerebral local oxygen metabolism.[59]

Validation of the three-phase model in future research

Although the influence of recirculating metabolic water is substantial, depending on the regional and global organism rates, the three-phase model accounts accurately for the metabolic rate differences between tissue types. Our measurements used long inhalation times of over 15 min, thus, requiring a non-linear metabolic model.[2] It can also be concluded that the longer duration of the inhalation phase does not linearly increase the $CMRO_2$ measurement sensitivity: it is limited by the accumulation of recirculating total body $H_2{}^{17}O$.

An internal ROI validation confirmed whether the voxels selected truly reflected the chosen tissue type by assessment of T_2* against metabolic rate in brain and muscle. Figure 5 shows a plot of the independent properties of tissue T_2* and metabolic rate values for the ROIs taken from muscle and brain under the two different ^{17}O MRS imaging protocols (low versus high spatial resolution protocol). Two well-separated clusters associated with the two types of tissues because of stark difference in transverse relaxation between the tissues (a much longer T_2* in brain than that of muscle)[22] confirm the placement, especially the muscle ROI covered sufficiently accurate the temporalis muscle. It also shows the fact that the strong divergence in metabolic rate is reflecting an underlying tissue difference. However, this approximate separation is only possible because of the significantly shorter T_2* value of $H_2{}^{17}O$ in muscle than that of brain tissue.[22]

It also has to be noted that certain metabolic rate variability stems from tissue heterogeneity within ROIs. For example, in the case of brain tissue estimates, despite low intra-session variance (e.g., see rat A) a hemispheric difference was likely induced through ROI choice near the boundary between brain and muscle tissues leading to partial volume effects. Another technical limitation is the relatively low SNR of ^{17}O signal detected in the muscle due to short T_2*,[22] and lateral differences in B_1 resulting in ~half SNR than that of brain tissue (see the ^{17}O spectra in Figures 2A and 2B). Therefore, the fidelity in imaging muscle could be improved, for instance, by using a coil array covering both brain and muscle with optimal detection sensitivity.

Finally, we would anticipate smaller variations of the ^{17}O MRSI approach when potentially activating the muscle by stimulation, as was done in a different paradigm during varying workload for instance, in cardiac muscle,[8,10] resulting in an elevated oxygen metabolic rate. In previous brain experiments, with an implantable ^{17}O RF coil, the measurement of an arterial input function and the measurement of blood flow through $H_2{}^{17}O$ bolus measurements was used for a detailed investigation, which also allowed the calculation of oxygen extraction fraction (OEF).[3] Thus, in future studies in other rat muscles (e.g., in the leg, by implantation of an arterial ^{17}O RF coil on the femoral artery or separately on the tail artery) the metabolic rate could be validated after electrical stimulation over a wide range of metabolic rates and perfusion. Dynamically measuring the increased metabolic rate during $^{17}O_2$ inhalations, could give new insights to different muscle fiber types. Furthermore, we

would expect a simultaneous measurement to be robust in consideration of systemic changes in animal physiology.

Conclusion

In this study, we have extended the applicability of in vivo ^{17}O MR imaging to measure and image the resting skeletal muscle with a very low oxygen metabolic rate (~16% of the brain tissue). We have also confirmed the consistency of the $CMRO_2$ results measured during prolonged and repeated inhalations of $^{17}O_2$ gas in this study with previous findings. Since the brain has a very high metabolic rate of oxygen consumption, in contrast to the very low rate in the resting muscle, we anticipate that the same ^{17}O MR imaging approach and modeling will be useful for other organs such as liver and heart. Therefore, we expect a broad impact of using the ^{17}O MR imaging technology for metabolic rate measurements in normal and diseased organs beyond the brain.

Supplementary Material

Refer to Web version on PubMed Central for supplementary material.

Acknowledgements:

The study was sponsored by the Max Planck Society and in part by the NIH grants: R01 NS070839, R01 MH111413, R01 CA240953, U01 EB026978 and P41 EB027061 and by the Institute for Basic Science, Suwon, Republic of South Korea (IBS-R015-D1) to Kâmil Uludağ.

REFERENCES

1. Zhu X-H, Chen W. In vivo ^{17}O MRS imaging – Quantitative assessment of regional oxygen consumption and perfusion rates in living brain. Anal Biochem. 2017;529:171–178. doi:10.1016/j.ab.2016.08.026 [PubMed: 27568551]
2. Atkinson IC, Thulborn KR. Feasibility of mapping the tissue mass corrected bioscale of cerebral metabolic rate of oxygen consumption using 17-oxygen and 23-sodium MR imaging in a human brain at 9.4 T. Neuroimage. 2010;51(2):723–733. doi:10.1016/j.neuroimage.2010.02.056 [PubMed: 20188194]
3. Zhu X-H, Zhang Y, Tian R-X, et al. Development of ^{17}O NMR approach for fast imaging of cerebral metabolic rate of oxygen in rat brain at high field. Proc Natl Acad Sci U S A. 2002;99(20):13194–13199. doi:10.1073/pnas.202471399 [PubMed: 12242341]
4. Zhu X, Zhang Y, Ugurbil K, Chen W. 3D Imaging of $CMRO_2$ in Rat Brain at Different Temperature using High-field ^{17}O NMR Approach. In Proceedings of the 11th Annual Meeting of ISMRM, Toronto, Canada 2003 p. 569.
5. Zhu X-H, Zhang N, Zhang Y, Ugurbil K, Chen W. New insights into central roles of cerebral oxygen metabolism in the resting and stimulus-evoked brain. J Cereb Blood Flow Metab. 2008;29(1):10–18. doi:10.1038/jcbfm.2008.97 [PubMed: 18781163]
6. Hoffmann SH, Begovatz P, Nagel AM, et al. A measurement setup for direct ^{17}O MRI at 7 T. Magn Reson Med. 2011;66(4):1109–1115. doi:10.1002/mrm.22871 [PubMed: 21394777]
7. Niesporek SC, Umathum R, Lommen JM, et al. Reproducibility of $CMRO_2$ determination using dynamic ^{17}O MRI. Magn Reson Med. 2018;79(6):2923–2934. doi:10.1002/mrm.26952 [PubMed: 29030876]
8. Lu M, Atthe B, Mateescu GD, Flask CA, Yu X. Assessing mitochondrial respiration in isolated hearts using ^{17}O MRS. NMR Biomed. 2012;25(6):883–889. doi:10.1002/nbm.1807 [PubMed: 22161858]

9. Borowiak R, Groebner J, Haas M, Hennig J, Bock M. Direct cerebral and cardiac ^{17}O-MRI at 3 Tesla: initial results at natural abundance. MAGMA. 2014;27(1):95–99. doi:10.1007/s10334-013-0409-0 [PubMed: 24077796]
10. Zhu X-H, Zhang Y, Chen W. In Vivo ^{17}O MRS Imaging for Assessing Myocardial Oxygen Metabolism in Rat Heart at 9.4T. In Proceedings of the 18th Annual Meeting of ISMRM, Stockholm, Sweden, 2010 p. 172.
11. Zhu X-H, Zhang Y, Zhang N, Ugurbil K, Chen W. Noninvasive and three-dimensional imaging of $CMRO_2$ in rats at 9.4T: reproducibility test and normothermia/hypothermia comparison study. J Cereb Blood Flow Metab. 2006;27(6):1225–1234. [PubMed: 17133228]
12. Zhu X-H, Zhang Y, Wiesner HM, Ugurbil K, Chen W. In vivo measurement of CBF using ^{17}O NMR signal of metabolically produced $H_2{}^{17}O$ as a perfusion tracer. Magn Reson Med. 2013:70:309–314. doi:10.1002/mrm.24469 [PubMed: 23001743]
13. Irving CS, Lapidot A. Haemoglobin-$^{17}O_2$ Revisited. Nature. 1971;230(15):224–224. doi:10.1038/10.1038/newbio230224a0
14. Frackowiak R, Lenzi G-L, Jones T, Heather J. Quantitative Measurement of Regional Cerebral Blood Flow and Oxygen Metabolism in Man Using ^{15}O and Positron Emission Tomography: Theory, Procedure, and Normal Values. J Comput Assist Tomogr. 1980;4(6):727–736. [PubMed: 6971299]
15. Lammertsma AA, Jones T. Correction for the Presence of Intravascular Oxygen-15 in the Steady-State Technique for Measuring Regional Oxygen Extraction Ratio in the Brain: 1. Description of the Method. J Cereb Blood Flow Metab. 1983;3(4):416–424. doi:10.1038/jcbfm.1983.67 [PubMed: 6630313]
16. Mintun MA, Raichle ME, Martin WRW, Herscovitch P. Brain Oxygen Utilization Measured with O-15 Radiotracers and Positron Emission Tomography. J Nucl Med. 1984;25(2):177–187. [PubMed: 6610032]
17. Yang B, Verbavatz J-M, Song Y, et al. Skeletal muscle function and water permeability in aquaporin-4 deficient mice. Am J Physiol Cell Physiol. 2000;278(6):C1108–C1115. doi:10.1152/ajpcell.2000.278.6.C1108 [PubMed: 10837338]
18. Mitchell HH, Hamilton TS, Steggerda FR, Bean HW. The Chemical Composition of the Adult Human Body and Its Bearing on the Biochemistry of Growth. J Biol Chem. 1945;158(3):625–637.
19. Urbanchek MG, Picken EB, Kalliainen LK, Kuzon WM. Specific Force Deficit in Skeletal Muscles of Old Rats Is Partially Explained by the Existence of Denervated Muscle Fibers. J Gerontol A Biol Sci Med Sci. 2001;56(5):B191–B197. doi:10.1093/gerona/56.5.B191 [PubMed: 11320099]
20. Siesjö BK. Brain Energy Metabolism. New York: John Wiley & Sons; 1978.
21. Kurzhunov D, Borowiak R, Hass H, et al. Quantification of oxygen metabolic rates in Human brain with dynamic ^{17}O MRI: Profile likelihood analysis. Magn Reson Med. 2017;78(3):1157–1167. doi:10.1002/mrm.26476 [PubMed: 27804163]
22. Wiesner HM, Balla DZ, Shajan G, et al. ^{17}O relaxation times in the rat brain at 16.4 tesla. Magn Reson Med. 2016;75(5):1886–1893. doi:10.1002/mrm.25814 [PubMed: 26098931]
23. Pohmann R, von Kienlin M, Haase A. Theoretical Evaluation and Comparison of Fast Chemical Shift Imaging Methods. J Magn Reson. 1997;129(2):145–160. doi:10.1006/jmre.1997.1245 [PubMed: 9441879]
24. Brown TR, Kincaid BM, Ugurbil K. NMR chemical shift imaging in three dimensions. Proc Natl Acad Sci U S A. 1982;79(11):3523–3526. doi:10.2307/12315 [PubMed: 6954498]
25. Garwood M, Schleich T. Improved Fourier series windows for localization in in vivo NMR spectroscopy. J Magn Reson. 1985;65(3):510–515.
26. Pohmann R, von Kienlin M. Accurate phosphorus metabolite images of the human heart by 3D acquisition-weighted CSI. Magn Reson Med. 2001;45(5):817–826. doi:10.1002/mrm.1110 [PubMed: 11323808]
27. Paxinos G, Watson C. The Rat Brain in Stereotaxic Coordinates: Hard Cover Edition. Academic Press; 2006.
28. Schumacher GH, Rehmer H. [On some differences in the chewing apparatus of Lagomorpha and Rodentia]. Anat Anz. 1962;111:103–122. [PubMed: 13909572]

29. Korfage JAM, Koolstra JH, Langenbach GEJ, van Eijden TMGJ. Fiber-type Composition of the Human Jaw Muscles—(Part 1) Origin and Functional Significance of Fiber-type Diversity. J Dent Res. 2005;84(9):774–783. doi:10.1177/154405910508400901 [PubMed: 16109984]
30. Tanaka E, Sano R, Kawai N, et al. Regional differences in fiber characteristics in the rat temporalis muscle. J Anat. 2008;213(6):743–748. doi:10.1111/j.1469-7580.2008.00990.x [PubMed: 19094190]
31. Cox PG, Jeffery N. Reviewing the Morphology of the Jaw-Closing Musculature in Squirrels, Rats, and Guinea Pigs with Contrast-Enhanced MicroCt. Anat Rec. 2011;294(6):915–928. doi:10.1002/ar.21381
32. Schütte E, Günther Th, Dulce HJ. Studien über den wasser- und salzhaushalt: III. Der wasser- und salzhaushalt von adrenalektomierten ratten bei kochsalzbelastung. Clin Chim Acta. 1958;3(6):557–564. doi:10.1016/0009-8981(58)90008-1 [PubMed: 13608870]
33. Sréter FA, Woo G. Cell water, sodium, and potassium in red and white mammalian muscles. Am J Physiol. 1963;205(6):1290–1294. doi:10.1152/ajplegacy.1963.205.6.1290 [PubMed: 14085002]
34. Sjogaard G, Saltin B. Extra- and intracellular water spaces in muscles of man at rest and with dynamic exercise. Am J Physiol Regul Integr and Comp Physiol. 1982;243(3):R271–R280. doi:10.1152/ajpregu.1982.243.3.R271
35. Zhu X-H, Chen JM, Tu T-W, Chen W, Song S-K. Simultaneous and noninvasive imaging of cerebral oxygen metabolic rate, blood flow and oxygen extraction fraction in stroke mice. Neuroimage. 2013;64:437–447. doi:10.1016/j.neuroimage.2012.09.028 [PubMed: 23000789]
36. Zhang N, Zhu X-H, Lei H, Ugurbil K, Chen W. Simplified Methods for Calculating Cerebral Metabolic Rate of Oxygen Based on ^{17}O Magnetic Resonance Spectroscopic Imaging Measurement During a Short $^{17}O_2$ Inhalation. J Cereb Blood Flow Metab. 2004;24(8):840–848. doi:10.1097/01.WCB.0000125885.54676.82 [PubMed: 15362714]
37. Heinonen I, Saltin B, Kemppainen J, et al. Skeletal muscle blood flow and oxygen uptake at rest and during exercise in humans: a pet study with nitric oxide and cyclooxygenase inhibition. A J Physiol Heart Circ Physiol. 2011;300(4):H1510–H1517. doi:10.1152/ajpheart.00996.2010
38. Muzik O, Mangner TJ, Leonard WR, Kumar A, Janisse J, Granneman JG. ^{15}O PET Measurement of Blood Flow and Oxygen Consumption in Cold-Activated Human Brown Fat. J Nucl Med. 2013;54(4):523–531. doi:10.2967/jnumed.112.111336 [PubMed: 23362317]
39. Field J, Belding HS, Martin AW. An analysis of the relation between basal metabolism and summated tissue respiration in the rat. I. The post-pubertal albino rat. J Cell Comp Physiol. 1939;14(2):143–157. doi:10.1002/jcp.1030140202
40. Rolfe DF, Brand MD. Contribution of mitochondrial proton leak to skeletal muscle respiration and to standard metabolic rate. Am J Physiol Cell Physiol. 1996;271(4):C1380–C1389. doi:10.1152/ajpcell.1996.271.4.C1380
41. Hood DA, Gorski J, Terjung RL. Oxygen cost of twitch and tetanic isometric contractions of rat skeletal muscle. Am J Physiol Endocrinol Metab. 1986;250(4):E449–E456. doi:10.1152/ajpendo.1986.250.4.E449
42. Behnke BJ, Barstow TJ, Kindig CA, McDonough P, Musch TI, Poole DC. Dynamics of oxygen uptake following exercise onset in rat skeletal muscle. Respir Physiol Neurobiol. 2002;133(3):229–239. doi:10.1016/S1569-9048(02)00183-0 [PubMed: 12425970]
43. Hochachka PW. Muscles as Molecular and Metabolic Machines. Boca Raton: CRC Press; 1994.
44. Schiaffino S, Reggiani C. Molecular diversity of myofibrillar proteins: gene regulation and functional significance. Physiol Rev. 1996;76(2):371–423. [PubMed: 8618961]
45. Hensbergen E, Kernell D. Daily durations of spontaneous activity in cat's ankle muscles. Exp Brain Res. 1997;115(2):325–332. doi:10.1007/PL00005701 [PubMed: 9224860]
46. Koga S, Rossiter HB, Heinonen I, Musch TI, Poole DC. Dynamic Heterogeneity of Exercising Muscle Blood Flow and O_2 Utilization Med Sci Sports Exerc. 2014;46(5):860–876. doi:10.1249/MSS.0000000000000178 [PubMed: 24091989]
47. Pereira JAASA, Wessels A, Nijtmans L, Moorman AFM, Sargeant AJ. New method for the accurate characterization of single human skeletal muscle fibres demonstrates a relation between mATPase and MyHC expression in pure and hybrid fibre types. J Muscle Res Cell Motil. 1995;16(1):21–34. doi:10.1007/BF00125307 [PubMed: 7751402]

48. Korfage JAM, Koolstra JH, Langenbach GEJ, van Eijden TMGJ. Fiber-type Composition of the Human Jaw Muscles—(Part 2) Role of Hybrid Fibers and Factors Responsible for Inter-individual Variation. J Dent Res. 2005;84(9):784–793. doi:10.1177/154405910508400902 [PubMed: 16109985]
49. Anderson EJ, Neufer PD. Type II skeletal myofibers possess unique properties that potentiate mitochondrial H_2O_2 generation. Am J Physiol Cell Physiol. 2006;290(3):C844–C851. doi:10.1152/ajpcell.00402.2005 [PubMed: 16251473]
50. McCommis KS, He X, Abendschein DR, Gupte PM, Gropler RJ, Zheng J. Cardiac ^{17}O MRI: Toward direct quantification of myocardial oxygen consumption. Magn Reson Med. 2010;63(6):1442–1447. doi:10.1002/mrm.22382 [PubMed: 20512845]
51. Mateescu GD, Fercu D. Interleave $^{17}O/^{31}P$ MRS: novel approach for in vivo determination of defects in oxidative phosphorylation (mitochondrial metabolism). In Proceedings of the 12th Annual Meeting of SMRM, New York, NY, USA 1993 Abstract 110.
52. Mateescu GD, Cabrera ME. In vivo ^{17}O magnetic resonance spectroscopy. Determination of temperature effects on metabolic rates (Q10 factor) In: Nemoto EM et al. (eds) Oxygen Transport to Tissue XVIII. Advances in experimental medicine and biology. vol 411 Boston: Springer; 1997 p 585–590.
53. Turek Z, Kreuzer F, Ringnalda B. Blood gases at several levels of oxygenation in rats with a left-shifted blood oxygen dissociation curve. Pflugers Arch. 1978;376(1):7–13. doi:10.1007/BF00585241 [PubMed: 568243]
54. Dawidson I, Eriksson BO, Gelin L-E, Soderberg R. Oxygen consumption and recovery from surgical shock in rats: a comparison of the efficacy of different plasma substitutes. Crit Care Med. 1979;7(10):460. [PubMed: 477354]
55. Lighton JR. Measuring Metabolic Rates: A Manual for Scientists: A Manual for Scientists. Oxford: Oxford University Press; 2008.
56. Meyer CW, Willershäuser M, Jastroch M, et al. Adaptive thermogenesis and thermal conductance in wild-type and UCP1-KO mice. Am J Physiol Regul Integr and Comp Physiol. 2010;299(5):R1396–R1406. doi:10.1152/ajpregu.00021.2009 [PubMed: 20826705]
57. Speakman JR. Measuring Energy Metabolism in the Mouse – Theoretical, Practical, and Analytical Considerations. Front Physiol. 2013;4. doi:10.3389/fphys.2013.00034
58. Hansen TD, Warner DS, Todd MM, Vust LJ. EFFECTS OF NITROUS OXIDE AND VOLATILE ANAESTHETICS ON CEREBRAL BLOOD FLOW. Br J Anaesth. 1989;63(3):290–295. doi:10.1093/bja/63.3.290 [PubMed: 2803887]
59. Myles PS, Leslie K, Peyton P, et al. Nitrous oxide and perioperative cardiac morbidity (ENIGMA-II) Trial: Rationale and design. Am Heart J. 2009;157(3):488–494.e1. doi:10.1016/j.ahj.2008.11.015 [PubMed: 19249419]
60. Oikonen V, Nuutila P, Sipilä H, Tolvanen T, Peltoniemi P, Ruotsalainen U. Quantification of oxygen consumption in skeletal muscle with PET and oxygen-15 bolus. Eur J Nucl Med. 1998;25:1151.
61. Nuutila P, Peltoniemi P, Oikonen V, et al. Enhanced stimulation of glucose uptake by insulin increases exercise-stimulated glucose uptake in skeletal muscle in humans: studies using $[^{15}O]O_2$, $[^{15}O]H_2O$, $[^{18}F]$fluoro-deoxy-glucose, and positron emission tomography. Diabetes. 2000;49(7):1084–1091. doi:10.2337/diabetes.49.7.1084 [PubMed: 10909962]

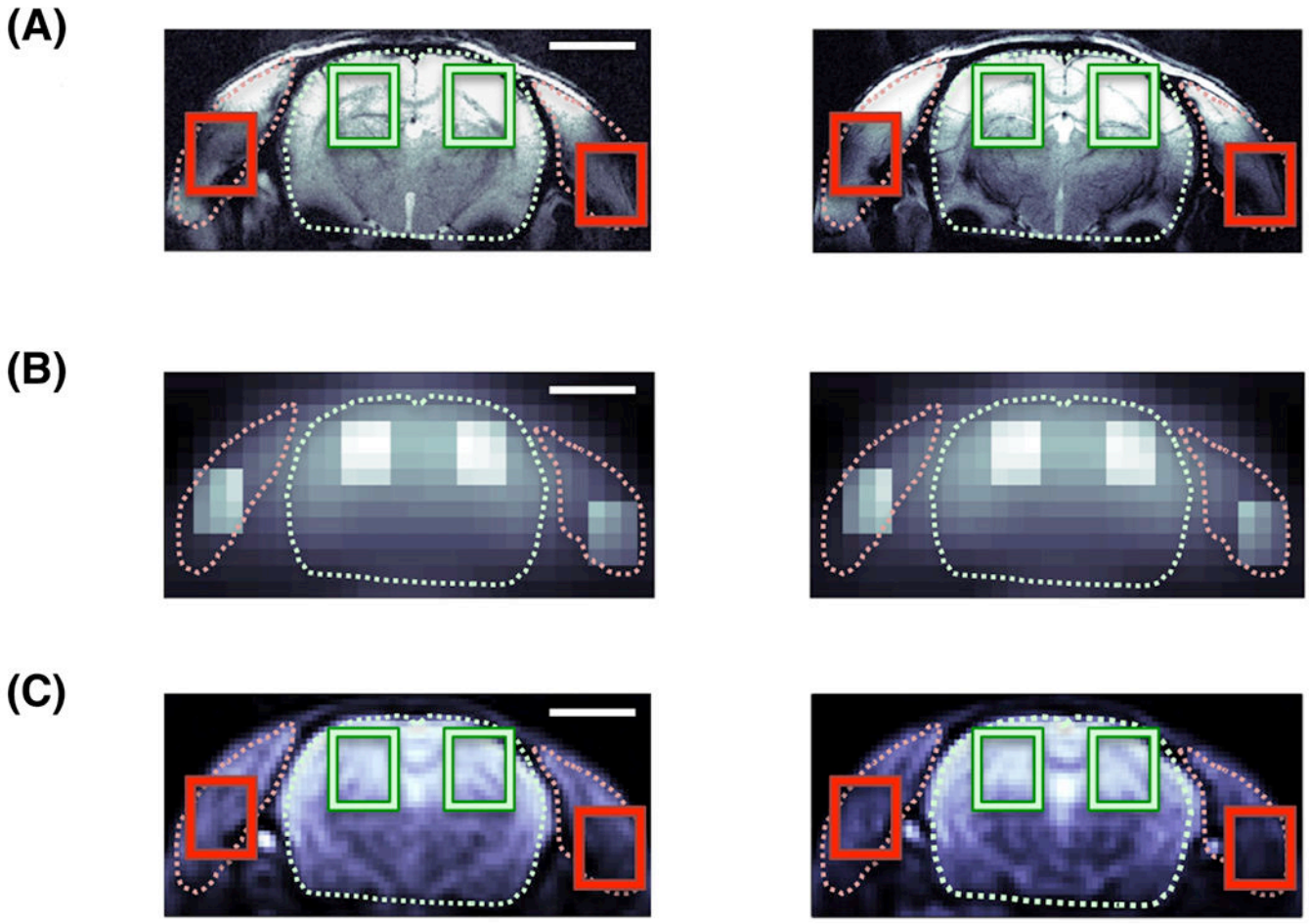

FIGURE 1.

Co-registered rat head images with 5mm scale bar: (A), ^{1}H FLASH structural image of the coronal rat head anatomy. Regions of interest (ROI) for brain tissue (green) are highlighted for each hemisphere and laterally left and right for muscle tissue (i.e. predominantly temporalis lateralis; red); (B), in vivo $H_2{}^{17}O$ image acquired within 30 s shortly before the onset of a $^{17}O_2$ inhalation, with intensity highlighting (2× brighter) of the ROIs for better visualization; and (C), very high resolution $H_2{}^{17}O$ enriched post-mortem image acquired after repeated inhalations with ROIs marked as in (A). All slices cover the same FOV at the Z-position of the Bregma. Visualization of brain and muscle (dotted line) based on proton images (A). ^{17}O images in (B,C) are zero-filled (×2) in the spatial dimensions.

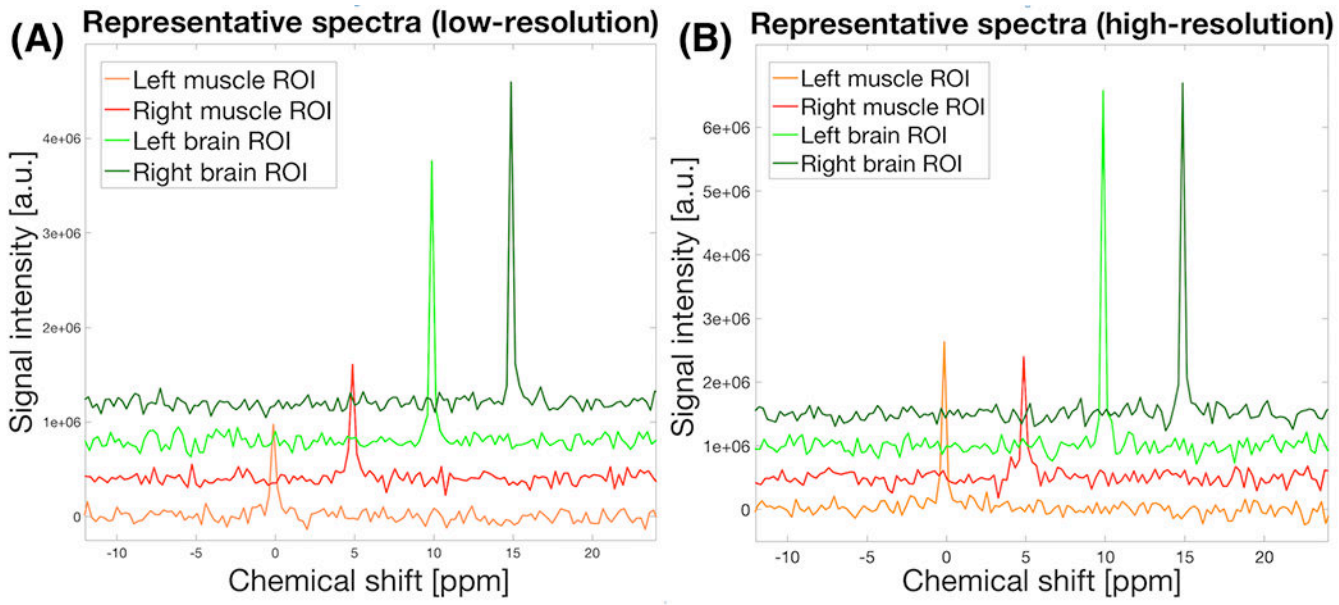

FIGURE 2.

Representative natural abundance $H_2{}^{17}O$ spectra summed over the brain and muscle ROIs in one CSI volume with: (A), lower spatial resolution (10 s acquisition averaging) and (B), higher spatial resolution (30 s acquisition averaging) protocol. Stacked displays of phase corrected spectra are shifted to the vertically and horizontally for visualization (Note, the $H_2{}^{17}O$ signal was heterogeneously affected in SNR because of the B_1 sensitivity profile of the two ^{17}O surface coils being used).

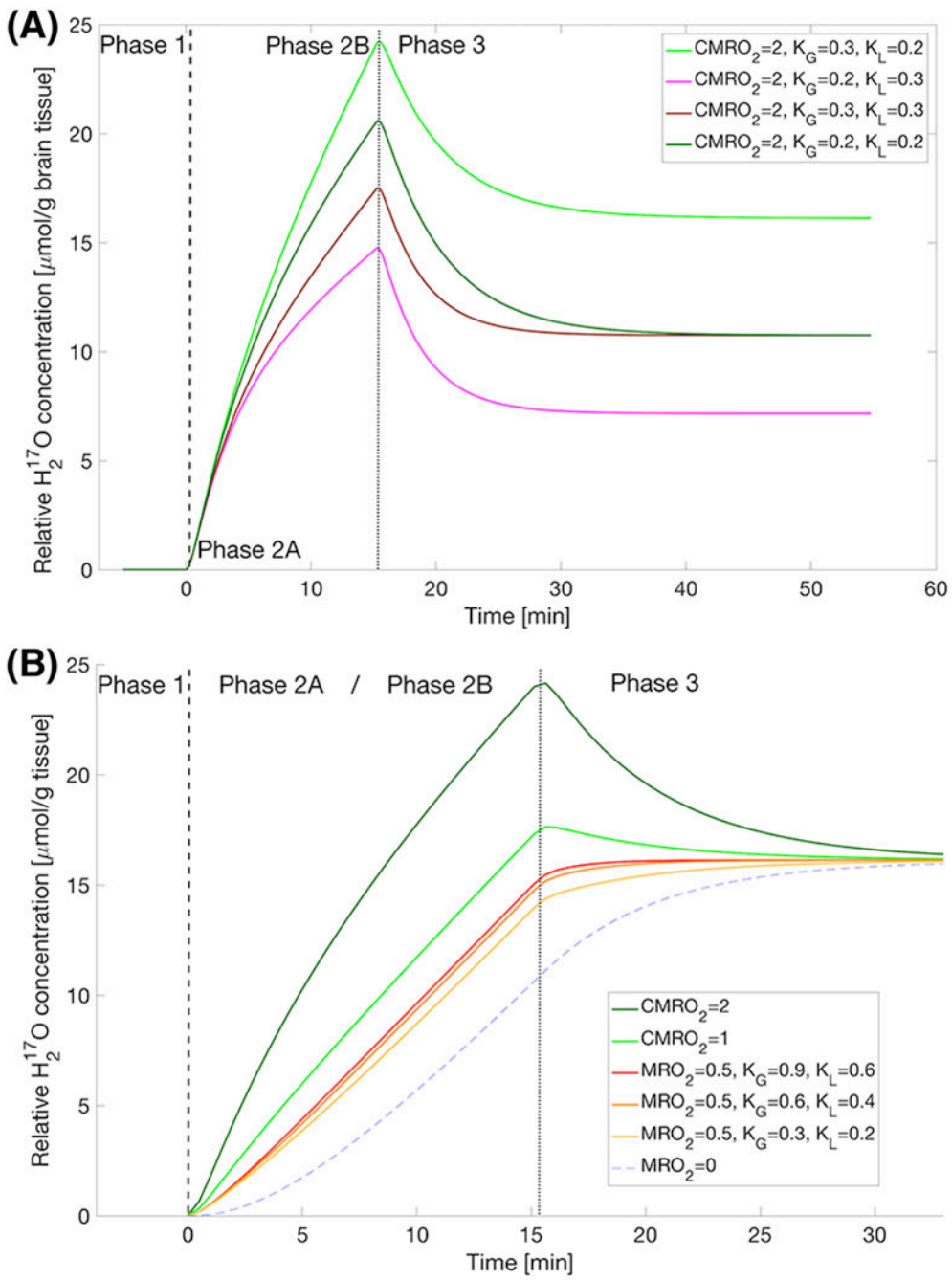

FIGURE 3.

(A) A simple iso-metabolic comparison of varying degrees of perfusion and circulatory parameters (i.e., the K_G and K_L parameter values) using the three-phase model (Eqn.[1]) highlighting phases in high metabolizing tissue: Phase 1 - pre-inhalation natural abundance $H_2{}^{17}O$; Phase 2 - during inhalation with initial increases dominated by locally produced $H_2{}^{17}O$ (Phase 2A as the first ~2-4 min) and subsequently varied slopes (especially in later Phase 2B) from the different perfusion and circulation parameters; Phase 3 – post-inhalation

$H_2{}^{17}O$ with varying washout rates to reach equilibrium levels that were linearly affected by the K_G / K_L ratio at the same local metabolic rate.

(B) Zoomed (~2x) in time three-phase model plots at different metabolic rates: during the first few minutes, the $H_2{}^{17}O$ water content in low metabolizing tissue increases much slower than that in the higher ones (Phase 2A), signals approach a similar slope during Phase 2B and at the end of the inhalation, the $H_2{}^{17}O$ in low metabolizing tissue continues to rise with gradually decreased slope; both high and low metabolizing tissue approach the same equilibrium due to recirculation of body water at a new steady-state level determined by the global metabolic rate (VO_2, according to Eqn. [2]). Unless otherwise stated in the legend, all time courses in (B) had K_G=0.3 and K_L=0.2.

The dashed and dotted lines indicate the beginning and end of the Phase 2, respectively.

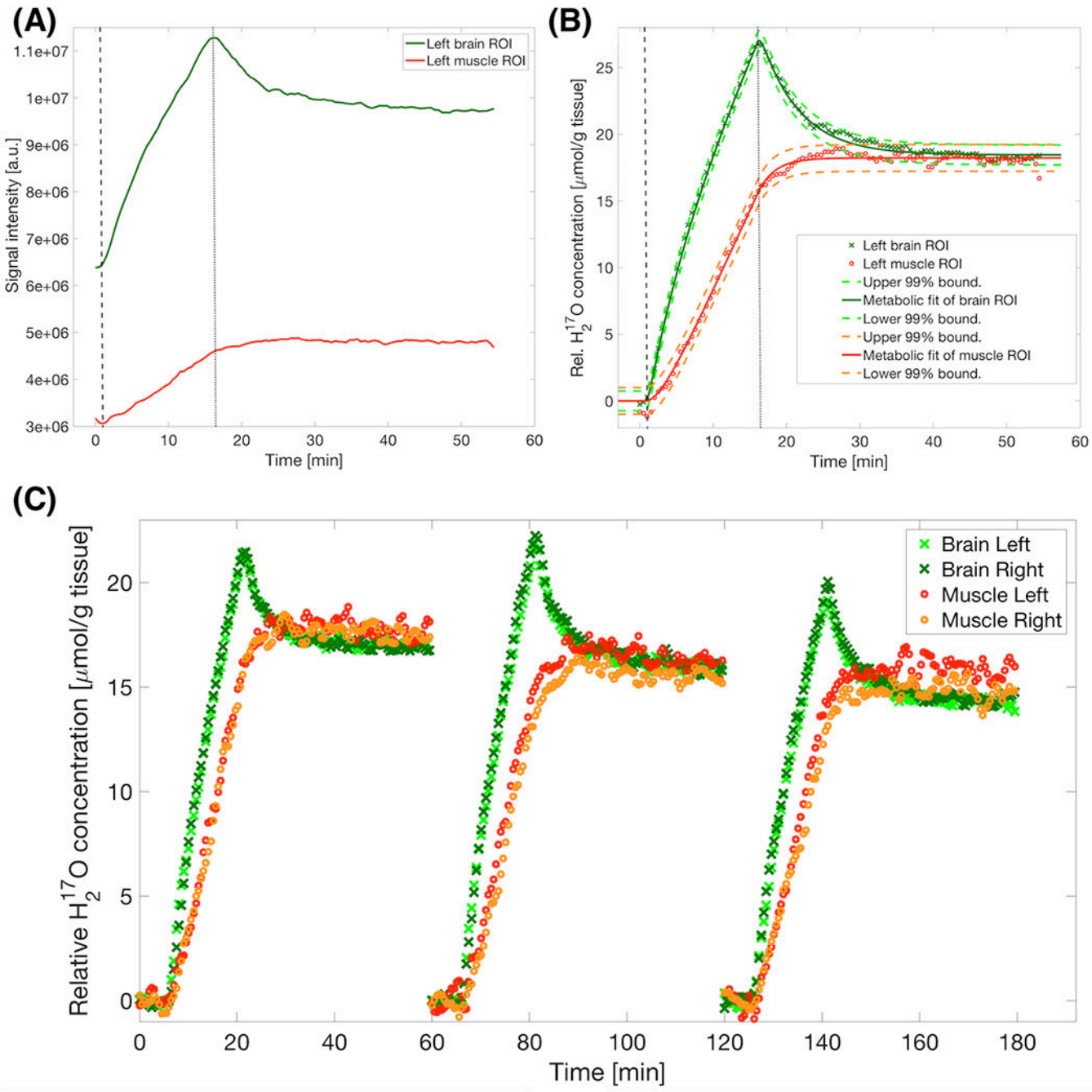

FIGURE 4.

(A) Time courses of raw $H_2{}^{17}O$ signal intensity in one representative rat during and after a 15-minute inhalation of $^{17}O_2$ gas in ROIs of brain (green) and muscle (red) tissues; and (B) post-processed molar $H_2{}^{17}O$ concentration time courses of the same data. The dashed and dotted vertical lines highlight the beginning and end of the $^{17}O_2$ inhalation. Non-linear least-square fits of the three-phase metabolic model (continuous lines) yielded a brain $CMRO_2$ of 1.94 μmol/g tissue/min and muscle $RMRO_2$ of 0.32 μmol/g tissue/min. An equilibrium value of around 17 μmol/g tissue over the pre-inhalation $H_2{}^{17}O$ concentration in both tissue types

was confirmed by matching 99% prediction bounds of the fit (dashed surrounding lines). The baseline $H_2{}^{17}O$ concentration was set at zero, which was above natural abundance level due to a prior $^{17}O_2$ inhalation. Finally, a comparable fit quality was shown by the very similar spread of the confidence intervals despite their significantly different metabolic estimates. (C) Normalized display of multiple inhalations showing the reproducibility of the technique in the same animal. Note the reproducible convergence at the end of each inhalation time course despite the differences in metabolic rate. With longer experimental duration, maintaining stable anesthetic conditions becomes more challenging as also reflected in higher signal fluctuations.

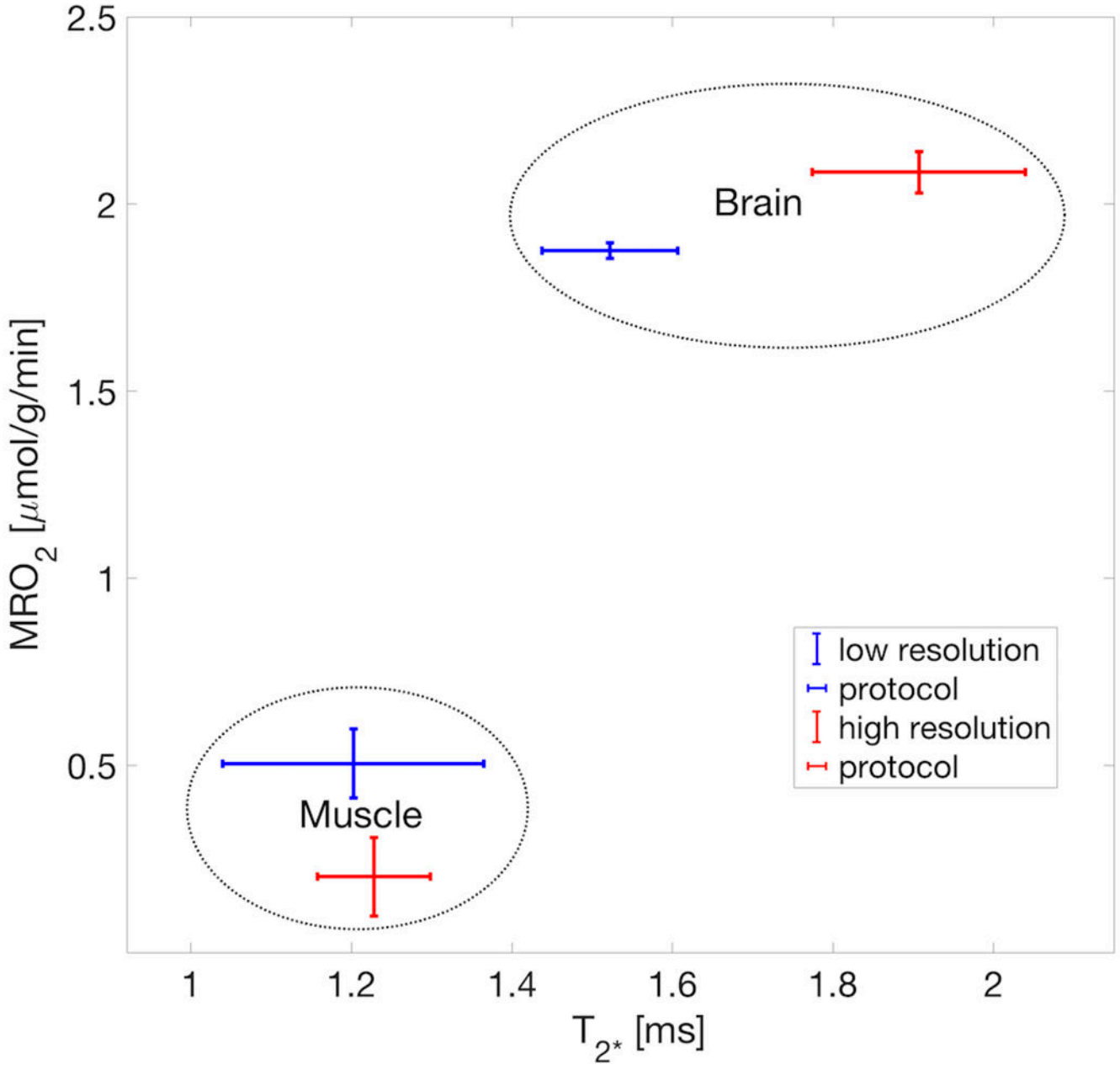

FIGURE 5.

Scatter plot of in-vivo tissue T_2* vs. metabolic rate showing high correlation in both tissue types of brain and muscle from clearly separated clusters of the independent properties of metabolic rate and relaxometric behavior inside ROIs. The distinction benefits from the fact of a stark difference in T_2* as also previously reported for both in vivo and post-mortem tissues. Each cluster is based on the pooled tissue type of two representative rats (rat A and rat G), of each high resolution and low resolution protocols, respectively. Note: this is only an observation to confirm the accurate selection and size (i.e. partial volume contamination)

of the ROIs and does not imply a causal relation between relaxation rate and metabolic rate in either direction.

Table 1

Summary of performed inhalation numbers and inhalation durations and weight for each animal.

Individual animal	gas mixture	Body weight [g]	Inh. number	Inh. Duration [min]
rat A	N_2	300	#1	15.3
	N_2		#2	15.3
rat B	N_2	232	#1	15.3
rat C	N_2	275	#1	15.1
	N_2		#2	15.1
rat D	N_2	233	#1	15.1
	N_2		#2	12.9
rat E	N_2O	250	#1	15.4
	N_2O		#2	15.1
	N_2O		#3	15.1
rat F	N_2O	510	#1	15.1
rat G*	N_2O	332	#1	15
rat H*	N_2O	367	#1	15
Pop. Mean ± SD:		**312 ± 93 g**		**15 ± 0.6 min**

Each row represents one resting $^{17}O_2$ inhalation measurement, which for rats A, C, D and E was repeated multiple times within the same experimental session per animal.

Table 2

Summary of the oxygen metabolic rate (μmol/g tissue/min) results measured in brain and muscle based on region of interest (ROI) analysis

Individual animal	$RMRO_2$ Left muscle ROI	$RMRO_2$ Right muscle ROI	$CMRO_2$ Left S1 ROI	$CMRO_2$ Right S1 ROI
rat A	0.15	0.11	2.11	2.08
	0.35	0.20	2.14	2.01
rat B	0.28	0.43	2.03	1.90
rat C	0.27	0.30	2.02	2.08
	0.33	0.31	2.06	2.01
rat D	0.32	*	2.30	2.45
	0.37	*	1.85	1.96
Mean ± SD	**0.30 ± 0.07**	**0.27 ± 0.12**	**2.07 ± 0.14**	**2.07 ± 0.18**
rat E	0.45	0.34	1.82	1.77
	0.45	0.16	1.82	1.83
	0.46	0.42	1.68	1.74
rat F	0.13	*	2.14	2.08
rat G **	0.44	0.57	1.86	1.89
rat H **	0.34	0.20	1.80	1.69
Mean ± SD	**0.38 ± 0.11**	**0.34 ± 0.14**	**1.85 ± 0.15**	**1.83 ± 0.14**
Mean values of right and left ROIs:	**$RMRO_2$=0.32 ± 0.12 *** **		**$CMRO_2$=1.97 ± 0.19 *** **	

* No convergence of the fitting procedure.

** This subgroup of 2 animals was acquired at a higher temporal resolution (10s per 3D CSI volume) with the lower spatial resolution protocol.

*** $p < 0.01$ significant tissue-type difference between muscle and brain (paired t-test).

Table 3

Summary of $VO_{2,average}$ (μmol/g tissue/min) and cerebral blood flow (ml/g tissue/min) results based on washout in brain.

Individual animal	$VO_{2,average}$ Left & Right Muscle ROI	$VO_{2,average}$ Left & Right Brain ROI	CBF Left Brain ROI	CBF Right Brain ROI
rat A	1.17	1.19	0.27	0.27
	1.19	1.17	0.28	0.26
rat B	1.21	1.04	0.28	0.25
rat C	1.19	1.16	0.26	0.28
	1.06	1.09	0.31	0.28
rat D	1.39	1.37	0.30	0.30
	1.15	1.14	0.28	0.26
Mean ± SD	**1.19 ± 0.10** **	**1.17 ± 0.10** **	**0.28 ± 0.02** **	**0.27 ± 0.02** **
rat E	1.14	1.11	0.41	0.33
	1.03	1.05	0.34	0.25
	1.02	0.95	0.29	0.29
rat F	0.64	0.91	0.32	0.33
rat G *	1.17	1.13	0.32	0.32
rat H *	0.74	0.73	0.46	0.38
Mean ± SD	**0.96 ± 0.22** **	**0.98 ± 0.15** **	**0.36 ± 0.06** **	**0.32 ± 0.05** **
Overall average of both N_2 & N_2O	**$VO_{2,average}$ (n=13) 1.08 ± 0.20 μmol/g body/min**	**$VO_{2,average}$ (n=13) 1.08 ± 0.16 μmol/g body/min**	**CBF (n=26) 0.30 ± 0.05 ml/g tissue/min**	

* This subgroup of 2 animals was acquired at a higher temporal resolution (10s per 3D CSI volume) and with lower spatial resolution protocol.

** $p<0.05$ significant population difference between N_2 (rats A-D) and N_2O (rats E-H) groups (unpaired t-test).

Table 4

Muscle oxygen metabolic rate literature values based on various techniques in rats and humans.

Species / Technique	**Muscle MRO_2 μmol/g/min**	**Skeletal muscle type**	**Literature Reference**
Rat – perfused	0.65	Global muscle estimate	Field et. al. 1939 [39]
Rat – perfused	0.37	Hindquarter	Hood et. al. 1986 [41]
Rat - perfused	0.23	Hindquarter	Rolfe & Brand 1996 [40]
Rat – perfused	0.75	Spinotrapezius	Behnke et. al. 2002 [42]
Rat – this study	**0.32**	**Temporalis muscle**	-
Human – invasive ΔA/V	0.13	Whole Leg	Oikonen et. al. 1998 [60]
Human - $^{15}O_2$ inhalation PET	0.11	Whole Leg	Oikonen et. al. 1998 [60]
Human - $^{15}O_2$ inhalation PET	0.10	Whole Leg	Nuutila et. al. 2000 [61]
Human - $^{15}O_2$ inhalation PET	0.05	Whole Leg	Heinonen et. al. 2011 [37]

Comparison between selected muscle metabolism estimates using different techniques in rodents and humans, with the latter being more similar to the $^{17}O_2$ inhalation technique used in this study.